DIRBE Observations of the Zodiacal Light

William T. Reach
Universities Space Research Association
Code 685, NASA/GSFC, Greenbelt, MD 20771

Bryan A. Franz
Applied Research Corporation
Code 685.3, NASA/GSFC, Greenbelt, MD 20771

Thomas Kelsall
Code 685, NASA/GSFC, Greenbelt, MD 20771

Janet L. Weiland
General Sciences Corporation
Code 685.3, NASA/GSFC, Greenbelt, MD 20771

Abstract. The Diffuse Infrared Background Experiment (DIRBE) aboard the *Cosmic Background Explorer* (*COBE*) [1] mapped the entire sky redundantly in 10 wavebands at 1.25, 2.2, 3.5, 4.9, 12, 25, 60, 100, 140, & 240 μm. The scattering or thermal emission from interplanetary dust contributes significantly to the sky brightness in all 10 wavebands, dominating most. The sky brightness is modulated in time due to the changing viewing aspect of the DIRBE line of sight through the interplanetary dust cloud. A three-dimensional semi-physical model for the distribution, emission, and scattering of interplanetary dust was optimized to match the time-dependence of the sky brightness as observed by DIRBE. The method and results of this fitting procedure are described, as are the difficulties and some future prospects for disentangling the zodiacal light from other contributions to the diffuse infrared sky brightness.

INTRODUCTION

The zodiacal light is the dominant foreground at infrared wavelengths, and the DIRBE search for the cosmic infrared background radiation (CIBR) begins with its removal from the observed brightness. The infrared spectrum of the North Galactic Pole (NGP), together with the estimated contributions from zodiacal light, starlight, and the interstellar medium, is shown as a Figure in the contribution by Hauser (1995). The estimated fraction of the total brightness due to zodiacal light varies from about 2/3 in the near-infrared (1.25–3.5 μm) to more than 90% in the mid-infrared (4.9–60 μm). Even in the far-infrared the zodiacal contribution cannot be neglected; based on the results described below, 25% of the NGP brightness at 240 μm is zodiacal light. Based on current infrared background residuals, the limits on the total energy density of the extragalactic

[1] The National Aeronautics and Space Administration/ Goddard Space Flight Center (NASA/GSFC) is responsible for the design, development, and operation of the Cosmic Background Explorer (*COBE*). Scientific guidance is provided by the *COBE* Science Working Group. GSFC is also responsible for the development of the analysis software and for the production of the mission data sets.

infrared radiation field is dominated by the relatively poor limits in the mid infrared (Hauser 1995). Thus any cosmological processes that produce energy that is redshifted to this spectral region are only poorly constrained at present by infrared observations. It has been argued that limits to the extragalactic near- and mid-infrared radiation field from high-energy γ rays are much more stringent (cf. Stecker 1995). In order to limit the CIBR by direct observations, the zodiacal light has to be modeled to unprecedented precision.

This paper describes the observations and modeling of the zodiacal light by the Diffuse Infrared Background Experiment (DIRBE) science team. The goal of this work is to provide a method for subtracting the zodiacal light from DIRBE observations at 1.25 μm through 240 μm, preserving any isotropic component of the sky brightness and achieving $\sim$ 1% accuracy at high latitude. To this end, we created a three-dimensional model for the interplanetary dust cloud that predicts scattered sunlight and thermal emission, optimized parameters in the cloud model to match the modulated component of the observed brightness, and subtracted the model from the data to examine residuals for temporal and angular variations.

OBSERVATIONS

DIRBE is an absolutely calibrated photometer, with an accurate zero-brightness offset measurement in its 0.7° beam (Boggess *et al.* 1992). The gain calibration is stabilized using an internal reference source and non-variable celestial sources on short and long timescales, respectively (DIRBE Explanatory Supplement 1995; Mitchell *et al.* 1995). Absolute gain calibration was determined using observations of bright celestial sources. The absolute calibrator is Sirius from 1.25 to 12 μm, NGC 7027 for 25μm, Uranus for 60 and 100 μm, and Jupiter for 140 and 240 μm. Ideally, the same calibrator would be used at all wavelengths, but compromises were forced by the fact that Sirius becomes too faint at wavelengths longer than 12 μm and Jupiter is so bright that the 60 and 100μm detectors become nonlinear. For these reasons we have avoided using DIRBE as a spectrometer where possible, and our model includes free parameters for the gain in each waveband.

TABLE 1. Properties of the Diffuse Infrared Background Experiment

Band	1	2	3	4	5	6	7	8	9	10
Wavelength (μm)	1.25	2.2	3.5	4.9	12	25	60	100	140	240
Gain Uncertainty (%)	4	4	4	3	12	15	9	14	11	12
Offset Uncertainty(nW/m^{2}sr)	0.05	0.03	0.02	0.01	0.02	0.01	2	1	8	3
Gain Stability (%)	0.5	0.5	0.5	0.5	0.75	0.75	2	3	5	5

The combination of the orbit of the *COBE* satellite about Earth, spin of the DIRBE field of view about the satellite axis, and the orbit of the Earth around the Sun lead to a helical scan pattern on the sky. In one week, half the sky is fully sampled. The weekly sky maps are the basis for this work, as a compromise between using the full time-ordered data (which are too numerous) and using longer averaging times (which smear temporal variations of the zodiacal light). In formulating our goodness-of-fit criterion, we weighted each observation using a combination of a 'random' and 'systematic' error estimate. The random error estimate is based on the observed variation of brightness with time in each pixel

during the week. The systematic error is based on the estimated gain stability (listed in Table 1), determined from observations of a network of point sources throughout the mission.

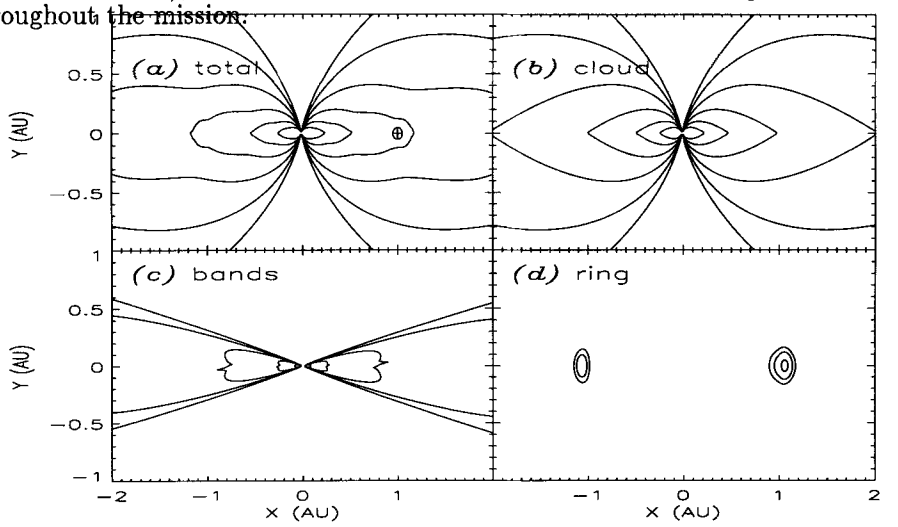

FIGURE 1. Density contours of our zodiacal cloud model. *(a)* total of all components; *(b)* 'smooth cloud'; *(c)* dust bands; *(d)* Earth's dust ring.

THREE-DIMENSIONAL MODEL FOR THE ZODIACAL CLOUD

The brightness of the zodiacal light is the integral along the line of sight of scattering and thermal contributions:

$$Z_\nu = \rho \int n(R,z,\theta)\{A_\nu F_\nu^\odot \Phi(\Theta) + (1-A_\nu)E_\nu B_\nu(T)\}\,\mathrm{d}s, \qquad (1)$$

where ρ is the volumetric extinction cross-section at 1 AU, A_ν is the albedo at frequency ν, $F_\nu^\odot$ is the solar flux, $\Phi(\Theta)$ is the phase function at scattering angle Θ, E_ν is the emissivity at frequency ν, and T is the grain temperature. The phase function is taken from previously published fits to the visible zodiacal light (Hong 1988), which are consistent with determinations using DIRBE data (Berriman *et al.* 1995). We assume the temperature varies with distance from the Sun as $T(R) = T_0 R^{-\delta}$. Throughout this paper, R is the distance from the Sun, z is the distance from the ecliptic plane.

The treatment of the albedos and emissivities is important for this work. We hope to achieve $\sim 1\%$ accuracy in removal of the zodiacal light from 1.25–240μm, but the accuracy of our calibration from waveband to waveband in the mid-infrared is relatively poor. Furthermore, it is unlikely that the assumption of a single grain temperature will apply with high accuracy. Models for the emission from interplanetary dust predict that a small range of temperatures contributes to the mid-infrared emission, expanding to a wider range at shorter wavelengths (Reach 1988). The wavelength-dependence of the albedo is essentially unknown, and a constant albedo is unlikely. In order to allow for the imprecision of the waveband-to-waveband calibration as well as the restrictive

nature of our spectral model, we allow the emissivities and albedos to be free parameters. There are three albedos (at 1.25, 2.2, & 3.5 μm) and 8 emissivities (at 3.5, 12, 25, 60, 100, 140, & 240 μm).

The cloud density is composed of 4 components,

$$n(R, z, \theta) = n_C + n_{B1} + n_{B2} + n_R,$$

each of which is shown in Figure 1 and discussed in turn below.

Smooth cloud model. The smooth cloud model is a cylindrical fan model, similar to that fitted to the *IRAS* data in producing the *IRAS Sky Survey Atlas* (Good *et al.* 1986; Good 1994):

$$n_C(r, z, \theta) = R_{xy}^{-\alpha} \exp(-\beta |z_c / R_{xy}|^{\gamma}), \tag{2}$$

where R_{xy} is the distance from the cloud center projected into the cloud midplane. The geometry is defined as follows. Let (x, y, z) be heliocentric Cartesian coordinates. The center is shifted from the Sun by (x_0, y_0, z_0), leading to the coordinates $(x', y', z') \equiv (x - x_0, y - y_0, z - z_0)$. The vertical distance from the midplane is then

$$z_c = x' \sin\Omega \sin i - y' \cos\Omega \sin i + z' \cos i, \tag{3}$$

where i and Ω are the inclination and ascending node of the dust midplane with respect to the ecliptic plane.

Dust bands. The dust bands were discovered in the *IRAS* data (Low *et al.* 1984), and are believed to be asteroidal collisional debris (Dermott *et al.* 1984; Sykes *et al.* 1989). The dust bands have been studied using the DIRBE data (Spiesman *et al.* 1995) confirming the observational results from *IRAS* data and extending them to the near-infrared. In particular, the parallactic and spectroscopic distances to the bands are less than the distance to the asteroid belt, so that the material producing them is likely to be debris spiralling into the Sun under Poynting-Robertson drag. For this work, we used a dust band density based on the migrating model (Reach 1992), but with a simpler analytic formulation that is easier to evaluate and optimize:

$$n_{Bi}(r, \zeta_{Bi}) = n_{1Bi} R^{-1} \exp\left[-\left(\zeta_{Bi}/\delta_{\zeta_{Bi}}\right)^6\right]\left[v_{Bi} + \left(\zeta_{Bi}/\delta_{\zeta_{Bi}}\right)^{p_{Bi}}\right], \tag{4}$$

where n_{1Bi} is the density at 1 AU, relative to that of the smooth cloud, of band i, $\zeta_{Bi} \equiv z_{Bi}/R$, z_{Bi} is the vertical distance from midplane of band i, and $\delta_{\zeta_{Bi}}, v_{Bi}, p_{Bi}$ are adjustable shape parameters. We included two bands, which appear at ecliptic latitudes around $\pm 10°$ and $\pm 1.4°$ in the sky maps and have been attributed (Sykes *et al.* 1989) to the Eos asteroid family ($\pm 10°$) and a blend of the Themis and Koronic families ($\pm 1.4°$).

Earth's dust ring. The Earth temporarily traps particles migrating asteroidal particles if they are in low-eccentricity orbits such as expected for asteroidal debris (Dermott *et al.* 1994; Dermott 1995). We have confirmed the existence of the Earth's dust ring by subtracting a smooth cloud model from two weekly sky maps, revealing the signature of the ring in remarkable agreement with the predictions (Reach *et al.* 1995). For this work, an empirical ring density model was developed to emulate the numerical simulations of Dermott *et al.* (1994).

It consists of a Gaussian (radial and vertical) toroid, with an enhancement in a 3-dimensional Gaussian blob trailing the Earth.

FITTING THE MODEL TO THE DATA

The infrared sky brightness is a combination of foregrounds due to interplanetary dust, starlight, and interstellar dust, as well as the CIBR. We will operationally define the CIBR to be an isotropic component of the sky brightness not associated with the abovementioned foregrounds. The problem at hand is to determine the contribution from interplanetary dust without modifying any of the other contributions. To this end, we use the one distinct signature of the zodiacal light: it is the only component that is not fixed on the celestial sphere. The brightness observed along a given celestial direction depends on the observer's line of sight with respect to the Sun on that day, as well as the position of the Earth in its orbit. The apparent time variation of the brightness toward two different directions is shown in Figure 2. Toward the ecliptic pole, the main causes for variation of the brightness are the motion of the Earth vertically, with respect to the inclined midplane of the dust distribution, as well as the motion of the Earth radially, due to its orbital eccentricity. At lower latitudes, the apparent temporal variation is primarily due to the changing solar elongation of the line of sight.

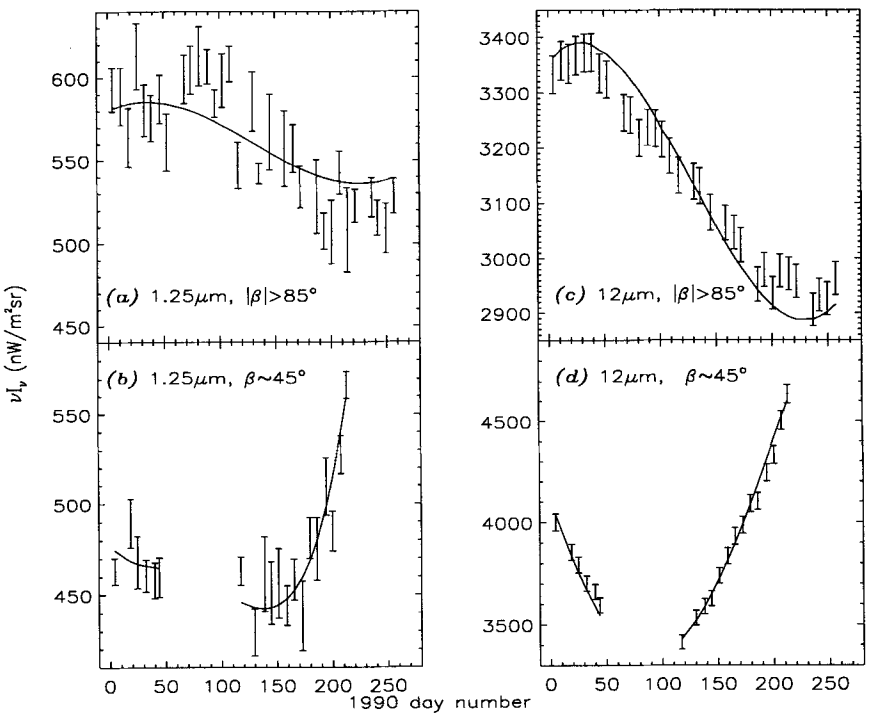

FIGURE 2. Observed brightness over the DIRBE mission for two directions in two wavebands. Error bars include random and systematic uncertainties.

We define the goodness of fit so that the model is optimized to match the modulation as follows. Let t be the observation time (an index over the weekly sky maps), p be the celestial position (an index over selected pixels), and b be the wavelength (an index over wavebands). The observed brightness is I_{tpb}, and the model evaluated for the same conditions is Z_{tpb}. Then we define the goodness of fit as

$$\chi^2[Z(t)] = \sum_{t,p,b} \left[(I_{tpb} - \langle I \rangle_{pb}) - (Z_{tpb} - \langle Z \rangle_{pb}) \right]^2 w_{tpb}. \quad (5)$$

In this equation, w_{tpb} is the weight given to an observation, which is based on a combination of random errors and the uncertainty in the temporal stability of the gain (Table 1). The mean brightness (over the mission) in each pixel is subtracted from both the model and the data. Therefore the sky brightnesses due to non-varying foregrounds and the CIBR are free parameters in this fitting method, with no assumptions about their morphology or spectrum.

The idea of using only the time variation to determine the zodiacal light was tested on simulated observations (including noise) of a model zodiacal cloud 'observed' by DIRBE. The above fitting procedure was able to recover the properties of the smooth cloud well. But for low-contrast features such as the dust bands and the Earth's dust ring, the time variation was inadequate to retrieve their shape. We therefore used a different method for part of the database. At 12 and 25 μm, and at absolute galactic latitude greater than 30°, the zodiacal light is the dominant sky brightness. If we assume all other contributions are isotropic, then we can define another goodness of fit,

$$\chi^2[Z + C] = \sum_{t,p,b} \left[(I_{tpb} - \langle I \rangle_b) - (Z_{tpb} - \langle Z \rangle_b) \right]^2 w_{tpb}, \quad (6)$$

where mean brightness *over the sky* was subtracted from each observation.

The total χ^2 for our fitting procedure is a combination of $\chi^2[Z + C]$ for the high-galactic latitude regions at 12 and 25 μm and $\chi^2[Z(t)]$ everywhere else. The parameters were determined using the Levenberg-Marquardt nonlinear least-squares optimization scheme (Bevington 1969). We selected 1920 lines of sight—one every $5° \times 5°$ patch of sky, and the total number of observations (including all wavebands and weekly samples) is 2×10^5. There are 30 model parameters as well as the free mean brightness in each pixel, which still leaves 1.8×10^5 degrees of freedom for the model fitting.

RESULTS

The fits to time strings are fairly 'good' in all wavebands, to within the accuracy of the DIRBE data as currently understood. The fit is shown together with the data in Figure 2 for selected individual pixels. The global goodness-of-fit χ^2/d.o.f. = 2.3 for the present model. While the fit appears excellent on a pixel-by-pixel basis, averages over patches large enough to reduce the random errors show some time variation in the residuals, which must be due to the zodiacal light. Maps of the total intensity, zodiacal light model, and residual intensity at 25 μm are shown in Figure 3. The residual maps at 1.25, 3.5, 12, & 60 μm are shown in Figure 2 of the contribution by Franz *et al.* (1995). Residual maps show that the bulk of angular variation that can be attributed to the zodiacal light is removed, but systematic residuals are clearly present

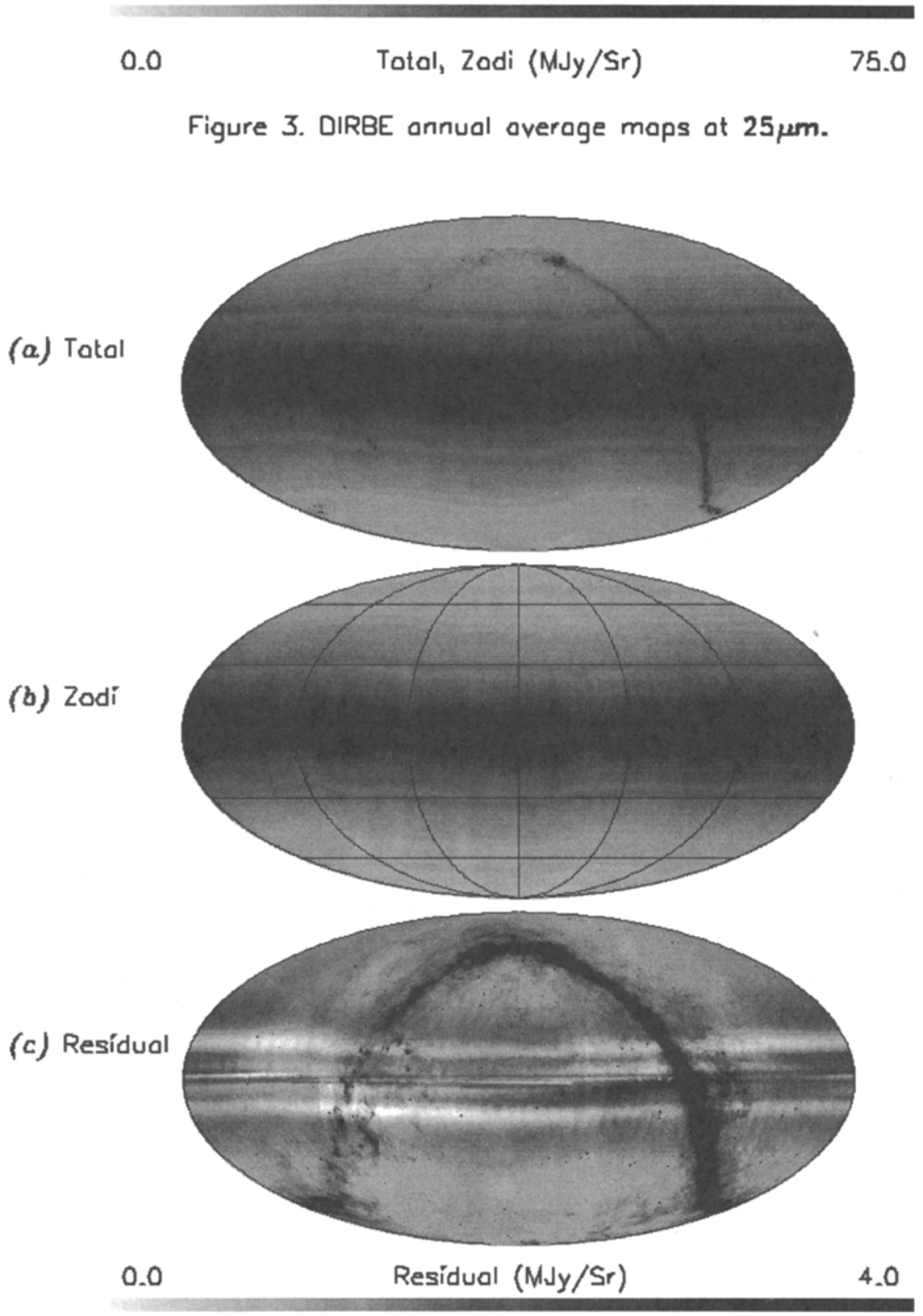

Figure 3. DIRBE annual average maps at 25μm.

in nearly every waveband. Curiously, the residual signature is nearly always positive near the ecliptic, which is to say there is a band of enhanced brightness there. We are experimenting with alternative formulations for the density of the 'smooth cloud' in order to determine whether the particular model presented here systematically biases the results toward positive residuals at higher ecliptic latitude, where the best limits to the cosmic infrared background are obtained.

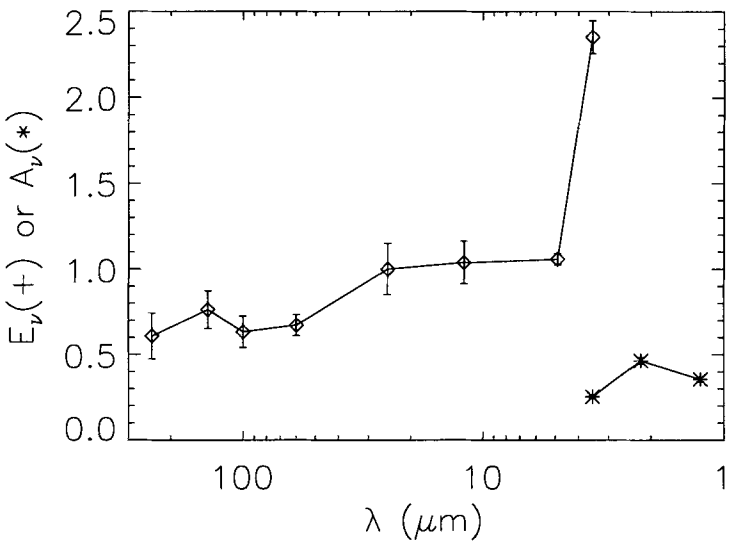

FIGURE 4. Emissivity ($\diamond$) and albedo (*) for each of the DIRBE wavebands for which they are determined. The error bars shown here include the absolute gain uncertainty.

Thermal emission from interplanetary dust was detected in 8 wavebands—including the first clear detection at 240 μm—and scattering was detected in 3 wavebands. The emissivities and albedos are shown in Figure 4. By our definition, the emissivities are normalized to unity at 25 μm. Ideal particles with radius a would be predicted to have an emissivity of unity at wavelengths $\lambda << 2\pi a$, and the emissivity would scale as a/λ at long wavelengths. We find that the emissivity is relatively flat through the mid-infrared and drops only modestly in the far-infrared. Based on the size distribution of interplanetary meteoroids (Grün *et al.* 1985), the particles that are expected to dominate the zodiacal light are large, with radii $\sim$ 30 μm (Reach 1988). Our observed slow rolloff of the emissivity in the far-infrared is consistent with such large particle sizes. On the other hand, the apparent emissivity enhancement at 3.5 μm is clearly not consistent with expectations based on physical optics and a single grain temperature. In principle, this feature could be due to a spectral line or other property of the grain material. A likely hypothesis is that the 3.5 μm emission, which is well into the Wien portion of the Planck function at the temperature (280 K)dominating the mid-infrared emission, is due to grains at temperatures $\gtrsim$ 400 K.

The fit we have obtained is already fairly 'good', despite systematic residuals, because we have removed the bulk of the time variation to within the systematic uncertainty in the DIRBE gain. Future improvements could arise from using a better functional form for the radial and vertical structure, using different fitting techniques, or relaxing some of the assumptions we have made about the interplanetary dust. Some of the assumptions that we will likely need to relax include the following:

1. The thermal emission is characterized by a greybody spectrum. This probably leads to the 'unphysical' 3.5 μm emissivity. Improvement of the spectral kernel, *e.g.* to include multiple temperatures, will not only make the emissivity variation with wavelength (Figure 4) more reasonable, but it may also lead to an improved fit to the angular dependence at 3.5 μm, which depends on the temperature more than in any other DIRBE waveband for which we have detected thermal emission.
2. The cloud is assumed to be plane-parallel. A warp is expected because the forced orbital elements depend on the semimajor axis of the orbit (Dermott 1995).
3. The phase function is assumed to be independent of wavelength. This is unlikely, as the scattering may be more isotropic at longer wavelengths. The albedos are also directly affected by the normalization of the phase function in equation (1). There has been an initial attempt to determine the phase function from the DIRBE data (Berriman *et al.* 1995).
4. Particle properties are assumed independent of location in the Solar System. The interplanetary dust consists of of asteroidal and cometary particles, which may have distinct properties. Further, structures such as the Earth's dust ring will have different size distributions due to size-dependent dynamical selection effects, and collision rates will vary throughout the Solar System. While these effects are hard to quantify, it may at least prove plausible to find different particle properties in the 'smooth cloud', dust bands, and Earth's ring.

Acknowledgements

For contributing ideas we acknowledge contributions from M. G. Hauser, C. M. Lisse, H. T. Freudenreich G. B. Berriman and the rest of the DIRBE science team.

References

Berriman, G. B., Weiland, J. L., Lisse, C. M., Reach, W. T., Hauser, M. G., & Kelsall, T. N. 1995, this workshop.

Bevington, P. R. 1969, *Data Reduction and Error Analysis for the Physical Sciences* (McGraw-Hill Inc.), pp 237-240.

Boggess, N. W., *et al.* 1992, ApJ, 397, 420

Dermott, S. F. 1995, this workshop.

Dermott, S. F., Nicholson, P. D., Burns, J. A., & Houck, J. R., 1984, Nature, 312, 505

Dermott, S. F., Jayraraman, S., Xu, Y. L., Gustafson, B. Å. S. & Liou, J. C. 1994, Nature, 369, 719

DIRBE Explanatory Supplement 1995, eds. M. G. Hauser *et al*, in preparation.

Franz, B. A., Reach, W. T., Kelsall, T., & Weiland, J. L. 1995, this workshop.

Good, J. C., Gautier, T. N. & Hauser, M. G. 1986, Adv. Space Res., 6, 84
Good, J. 1994, in *IRAS Sky Survey Atlas Explanatory Supplement*, ed. Wheelock, S. L. *et al.* JPL Publication 94-11 (Pasadena: JPL)
Grün, E., Zook, H. A., Fechtig, H., & Giese, R. H. 1985, Icarus, 62, 244
Hauser, M. G. 1995, this workshop.
Hong, S. S. 1988, A& Ap, 146, 67
Low, F. J. *et al.*, 1984, ApJ, 278, L19
Mitchell, K. J., Berriman, G. B., Kelsall, T., Richardson, D., Skard, J. A., & Stemwedel, S. W. 1995, this workshop.
Reach, W. T. 1988, ApJ, 335, 468
Reach, W. T. 1992, ApJ, 392, 289
Reach, W. T., Franz, B. A., Weiland, J. L., Hauser, M. G., Kelsall, T. N., Wright, E. L., Rawley, G., Stemwedel, S. W., & Spiesman, W. J. 1995, Nature, 374, 521
Spiesman, W. J., Hauser, M. G., Kelsall, T., Lisse, C. M., Moseley, S. H., Jr., Reach, W. T., Silverberg, R. F., Stemwedel, S. W. & Weiland, J. L. 1995, ApJ, 442, 662
Stecker, F. 1995, this workshop.
Sykes, M. V., Greenberg, R., Dermott, S. F., Nicholson, P. D., Burns, J. A., & Gautier, T. N., Jr. 1989, in *Asteroids II*, eds. R. P. Binzel, T. Gehrels, & Matthews (Tucson: U. Arizona), p. 336